Available online at www.sciencedirect.com
ScienceDirect
Journal of Power Sources 177 (2008) 434–450
JOURNAL OF POWER SOURCES
www.elsevier.com/locate/jpowsour

Modelling of fuel cells using multi-domain VHDL-AMS language

B. Blunier*, A. Miraoui

Université de Technologie de Belfort-Montbéliard, Rue Thierry Mieg, 90000 Belfort, France

Received 27 August 2007; received in revised form 9 October 2007; accepted 1 November 2007
Available online 9 January 2008

Abstract

This study presents a IEEE standard Very High Speed Integrated Circuit Hardware Description Language-Analog and Mixed-Signal Extension (VHDL-AMS) modelling of a complex multi-domain energy conversion system: a fuel cell stack. A comparative study between the different modelling approaches (bond graphs, electrical equivalent circuits) is given to show the great advantages of the VHDL-AMS language in the design process of fuel cell systems. The modelling approach allows the design team to split the work into several parts (concurrent engineering) and validate each part independently. The fuel cell stack model fits the experimental results. It is able to predict the voltage and the power of the fuel cell with a good accuracy taking into account the water content of the membrane. This last point is really important to design the air supply system (compressor and humidifier) and its associated control.

Keywords: Fuel cells; Energy conversion; Design methodology; Computer-aided engineering; Modelling; Hardware design languages

1. Introduction

Contemporary systems have become so complex that modelling became a part of the design process/cycle in order to validate functionality and performance of the whole system. For this purpose, system designers need a high-level perspective of the system. Fuel cells, or even more, fuel cell systems (FCS) are a good example of complexity, they include multi-domains continuous-time functionalities like electromechanical (e.g., electrical drives), electrical (e.g., power converter, electrical loads), electrochemical, fluidic (e.g., channels, compressor) and thermal parts [1]. They also include discrete-time functionalities for the control of such a complex system. A fuel cell system covers a range of modelling in different energy domains and spans levels of abstraction from low-level devices that make the components to the top-level functional unit. If we encompass such range of views of digital, analog and mixed-signal systems, the complexity we are dealing with is really high and it is not possible to comprehend such complex systems in their entirety without a proper methodology.

Methods which deal with the complexity have to be found in order to design, with some degree of confidence, components and systems that meet the requirements. Systematic methodology of design using a top-down design approach has to be applied [2]. This methodology decomposes the system design in a collection of components that interact which can be decomposed until a level where we have sufficient details [3]. Each component can have different levels of details (compromise between accuracy and performance) and abstraction. Each subsystem can be tested as part of the whole system and can be designed independently of others what facilitates concurrent engineering (e.g., one subsystem can be designed in one place, the other somewhere else) and improves productivity.

For this purpose Hardware Description Languages (HDLs) have been developed first for the electronic (digital) domain. Later on, Mixed-Signal Hardware Description Languages (MSHDLs) were created to be able to build complex models mixing analog and digital functionalities. These programming languages are used to develop executable simulation models of hardware systems, not only electrical systems but heterogeneous systems from several energy domains also called *multidisciplinary* or *mixed-disciplines* models [4]. The range of applications resulting from the capability of these powerful tools is astounding.

* Corresponding author.
E-mail addresses: benjamin.blunier@utbm.fr (B. Blunier), abdellatif.miraoui@utbm.fr (A. Miraoui).

0378-7753/$ – see front matter © 2007 Elsevier B.V. All rights reserved.
doi:10.1016/j.jpowsour.2007.11.002

Modern HDLs support both behavioural and structural mechanisms [3]. The first one allows the designer to express the operation of a subsystem at various levels of abstraction: from high abstract to very detailed levels. The second one, allows the designer to compose the model of a complete system from reusable model components stored in a library. Thus, in top-down design, an entire system, can contain some components with a high level of abstraction described behaviourally with little detail, another one can add, for example, parasitics and another one can decompose the component into lower level ones.

MSHDLs support both digital and analog functionalities. Digital functionality allows to model event-driven techniques and discrete time. Analog functionality allows to model systems of differential and algebraic equations (DAEs) where the solution varies continuously with time.

The needs for a mixed-signal simulation capability have resulted in the development of several proprietary languages like MAST by Analogy in 1986 and HLD-A by Mentor Graphics in 1992. The languages of these simulation environments are completely independent and the use and inter-operability are highly restricted: models developed for one system are not usable in other environments. Efforts to overcome these limitations have resulted in the development and standardisation of VHDL-AMS (IEEE standard Very High Speed Integrated Circuit Hardware Description Language-Analog and Mixed-Signal Extensions) presented hereafter. Another open language, Verilog-AMS (Open Verilog International) has to be mentioned but it did not receive standardisation yet. Interested readers can refer to [4] where a comparison between Verilog-AMS and VHDL-AMS is given in detail.

This article presents a VHDL-AMS model of a fuel cell stack. In the first part, the multi-domain modelling language, VHDL-AMS, is presented to introduce the language basic principles: interested readers will be able to find some good references to go forward. In a second part, a VHDL-AMS fuel cell stack model is presented after a comparison between the different modelling approaches which have been used in a great deal of papers (bond graphs, electrical equivalent circuits and signal flow). Finally, simulation and experimental results are presented: they show very good agreements. The last part concludes the work and gives the objectives and a roadmap to improve the model and build a *Functional Virtual Prototype* for the design and study of fuel cell systems.

2. Analysis and modelling

2.1. VHDL-AMS presentation

2.1.1. Overview

The IEEE 1076.1 language, informally known as VHDL-AMS, is a superset of IEEE Std 1076-1993 (VHDL) that provides capabilities for describing and simulating analog and mixed-signal systems with conservative and nonconservative semantics for the analog portion of the system. The language supports many abstraction levels in electrical and nonelectrical energy domains. The modelled analog systems are lumped systems that can be described by ordinary DAEs. The language does not specify any particular technique to solve the equations, but it rather defines the results that must be achieved. The solution of the equations may include discontinuities. Interaction between the digital part of a model and its analog part is supported in a flexible and efficient manner. Finally, support for frequency domain small-signal and noise simulation is provided [5].

The VHDL-AMS is designed to fill a number of needs in the process design [6]:

- it allows description of the structure of a system, that is, how it is decomposed into subsystems from different disciplines and how those subsystems are interconnected,
- it allows the specification of the function of a system using familiar programming language and equation forms,
- it allows the design of a system to be simulated before being manufactured: designers can compare alternatives and test for correctness without the delay and expense of hardware prototyping,
- it allows the detailed structure of a design to be synthesised from a more abstract specification, allowing designers to concentrate on more strategic design decisions and reducing time to market.

Moreover, the language is suited to express plant models and control algorithms needed for car manufacturers and suppliers [7]. In other words, it is able to communicate manufacturer's requests and supplier's solutions and it is suitable for model exchange within companies or between researchers and companies.

Several commercial simulators are available today like SystemVision (Mentor Graphics), Smash (Dolphin Integration), Simplorer (Ansoft) and SaberHDL (Synopsys).

2.1.2. Full working examples

In order to illustrate what is a VHDL-AMS language, a model of a resistor will be introduced. Using VHDL-AMS terminology, the module, or design entity is called `resistor` and the input and output are `ports`. Fig. 1 shows a VHDL-AMS description of the interface entity. This is an example of an *entity declaration*. The two first lines of the listing indicate that the entity involves of analog electrical-energy systems package. Then, the list of properties and parameters are defined. The resistor has one generic parameter, that is its resistance value. A default value of each generic parameter can be defined if it is required. The text after "–" are the comments and are not interpreted by the compiler. The `port` names `t1` and `t2` (line 11) are analog *terminals* port of the electrical nature, representing circuit nodes. A graphical representation of the resistor entity is given in Fig. 2. The electrical nature specifies that the terminal has voltage and current properties associated with it. This permits to connect the resistor to other terminals which are also of the electrical nature type.

The next step in building the model is to define the behavioural model of the resistor as shown in Fig. 3. Each terminal has to be associated with `across` and `through` branch quantities. This is done in line 2. For electrical nature, the pre-

```
1  library ieee;
2  use ieee.electrical_systems.all;
3
4  entity resistor is
5  -- generic model parameters
6   generic(
7     quantity R  : resistance := 1.0;
8         );
9  -- ports declaration
10  port(
11    terminal t1,t2 : electrical
12      );
13 end entity resisitor;
```

Fig. 1. VHDL-AMS resistor entity (interface) declaration.

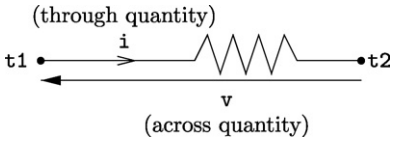

Fig. 2. Graphical representation of the VHDL-AMS resistor entity.

defined across type is voltage and the predefined through type is current.

Finally, a set of differential and algebraic equations (DAEs) can be written to describe the relations between the quantities. This is done with a *simultaneous statement* ("==") which has to be verified at each step of the simulation time. For the resistor, the simultaneous statement is straight forward: it is the ohmic law written in line 4.

```
1  architecture behav of resistor is
2    quantity v across i through t1 to t2;
3  begin
4     v == i*R;
5  end architecture behav;
```

Fig. 3. VHDL-AMS resistor architecture (behaviour) declaration.

```
1  library ieee;
2  use ieee.mechanical_systems.all;
3  use ieee.electrical_systems.all;
4  use ieee.math_real.all;
5
6  entity dcmp is
7    generic(
8      -- armature resistance
9      R   : resistance := 1.0;
10     -- armature inductance
11     L   : inductance := 0.01;
12     -- motor torque constant
13     K   : real := 1.0;
14     -- armature's moment of intertia
15     J    : moment_inertia := 0.075;
16     --- armature's damping
17     B    : damping := 0.0);
18   port(
19     -- electrical terminals
20     terminal t1, t2 : electrical;
21     -- mechanical terminal
22     -- rotational velocity nature
23     terminal m : rotational_v;
24     -- motor rotational speed in rpm
25     quantity N : out real;
26       );
```

Fig. 4. VHDL-AMS permanent magnet DC machine.

```
27 end entity dcmp;
28
29 architecture behav of dcmp is
30    constant om2n : real:=60.0/(2.0*math_pi);
31    quantity v across i through t1 to t2;
32    quantity Omega_m across T_m through m;
33 begin
34     -- elec. eq. :  V = R i + L di/dt + K Ω_m
35     v   == R*i+ L*i'dot+K*Omega_m;
36
37     -- mech. eq :  T_m = K i - J dΩ_m/dt - B Ω_m
38     T_m == K*i-J*Omega_m'dot-B*Omega_m;
39     N   == om2n*Omega_m;
40 end architecture behav;
```

Fig. 4. (*Continued*).

More complex models can be written and not only in the electrical domain. Fig. 4 shows a model of a permanent magnet DC machine which is an electro-mechanical device and has consequently both electrical and mechanical nature terminals. It has two electrical terminals (line 20) and one mechanical terminal (shaft) with a rotational-velocity nature (line 23). At the line 25, a type of port quantity is defined, the rotational speed of the motor defined as a `out` quantity. Quantities can either be declared as `in` or `out`. A graphical representation of the resistor entity is given in Fig. 5.

Simultaneous statements (lines 34–39) contain differential equations which are the well-known electrical and mechanical equations of a permanent DC machine. The time derivative of `x` is noted `x'dot`.

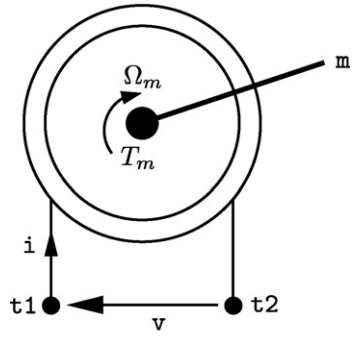

Fig. 5. Graphical representation of the VHDL-AMS DC machine entity.

It has to be noticed that the model does not assume which device is connected to the machine: the causes why the machine are rotating is not known *a priori*. Consequently, the model of the machine works in the four quadrants depending on if the voltage/current is imposed by a power converter or if the speed/torque is imposed by a mechanical load.

2.2. Fuel cell model

2.2.1. Fuel modelling approach review

Several modelling approaches have been used to model fuel cells: bond graphs, electrical equivalent circuits and signal flow. One of the first fuel cell multi-domain approach has been presented by Bernardi and Verbrugge [8] where the authors develop a one-dimensional steady state and isothermal fuel cell model. The model describes and predicts water transport, reactant species transport and ohmic and activation overpotential. Multi-domain approach involves derivation of a set of equations for each region of the fuel cell, that is gas diffusion regions (anode and cathode), gas flow channels, membrane and catalyst layer (anode and cathode): equations are solved separately and simultaneously [9]. A review and comparison of approaches for modelling PEM fuel cells have been done in [9,10]: interested readers can refer to these papers for more details. The aim of this part is to compare the three different approaches which are bond graphs, electrical equivalent circuit and signal flow.

2.2.1.1. Bond graph approach. Bond graphs are an explicit graphical tool for describing energy exchange within a system and facilitating multidisciplinary exchanges [11]. To this point of view, bond graphs and VHDL-AMS share advantages: they allow structural decomposition of the system into subsystems [12] and can also use a functional approach; bond graph like VHDL-AMS is unified for all physical domains [13,12] and can be easily connected to other existing models such as auxiliaries like other sources of energy, loads and power conversion devices.

They offer also a benefit on the control design: they have built-in causality assignment, an explicit definition of state variables and a direct graphic interpretation of controllability and observability in terms of causal paths. However, neither control scheme nor control strategies deduced from a fuel cell bond graphs model have been yet published: one can wonder if the complexity of the model itself does not permit to find easily control strategies. Even if bond graphs are a powerful tool, they also have some weaknesses. Firstly, they allow only energy exchanges which are described by bonds which represent power interaction: two variables *effort* and *flux* (equivalent to the variable *across* and *through* in VHDL-AMS) are associated with each bond. The power is calculated by multiplying effort and flux: for example in the fluidic domain, effort variable is the pressure (Pa) and flux is the volumetric flow rate (m^{-3} s). In some systems, like fuel cells, it would be more easy to use mass flow for mass conservation instead of volumetric flow but the product between a mass flow and a pressure does not give a power: therefore, volumetric flows are used for correct power calculation. Secondly, bond graphs, originally, do not support discontinuities: generally average models of power converter are

used where switching is not considered [11] and digital part of the system cannot be modelled (e.g., FPGA, digital controllers). Finally, the bond graph representation, even if it is powerful, cannot be easily read by a novice as contrasted with VHDL-AMS where physical equations are directly written, commented and possible to be understood by a novice.

2.2.1.2. Electrical equivalent circuits. In an attempt to support the modelling and simulation of nonelectrical as well, several modelling methods using energy equivalences between the electrical domain and other domains, such as mechanical, thermal, or fluidic domains, have been adopted. The basic method for creating a new model in a Spice-like environment is to combine pre-existing building blocks to achieve the desired functionality: voltage source, current controlled voltage sources [14], resistor, capacitance and even semi-conductors [15].

The electrical equivalent fuel cell models can be divided in two parts: the fuel cell electrical part model which contains only equivalent voltage sources, current-controlled voltages and resistor for activation, ohmic and concentration losses. The double layer charging effect is modelled by a capacitance. The most well-known simple equivalent circuit model have been presented and explained in many papers and books [16–19]. Other electrical equivalent circuit models have been presented and are summarised in [20]: most of them are mainly based on empirical results where parameters are identified by current interrupt technique or impedance spectrometry. However, empirical relationships do not provide an adequate physical understanding of the phenomena inside the cell.

Fuel cell gas channels have been modelled using equivalent electrical circuits. Mole or mass conservation of each species (H_2, H_2O, O_2) are modelled using three different electrical circuit where the voltage sources represent pressures, the current sources represent the flows [14,21]. Other components such as resistors and capacitor represents the fluidic resistance and capacitance of the channels. The model of Famouri and Gemmen [14] includes flow transients, reactant partial pressures and loss mechanisms within the fuel cell. Hernandez and Diong [21] takes into account some nonlinearities like the vapour saturation pressure but results show a divergent behaviour if the operating point zone migrates far away from the conditions used for model parameters identification because capacitances and resistances which are used in the model are constant. Wang et al. [22] developed also a complex dynamic fuel cell model using electrical analogies taking into account double layer charging effect and the thermodynamic characteristic inside the fuel cell. The Wang model has been successfully used in a distributed generation system model including power converters and control [23].

The electrical equivalent circuits have a greater limitation because they needs pre-defined buildings blocks. But what if the designer needs special effects for these models like temperature dependency? How about hydraulic or mechanical components that cannot be easily described with standard building block components? Designers may have several requirements that are possible to model using pre-defined building blocks. Moreover, while the function can be realised in this manner, it is rather hard to parameterise and reconfigure if needed: working with this type of macromodel can be a real limitation to system designer who needs a model quickly.

2.2.1.3. Signal flows. Signal flows modelling is the most used approach in control-oriented models: many fuel cell models have been published using Matlab/Simulink environment. Lukas et al. [24] developed a control-oriented dynamic simulation model of a direct reforming molten carbonate fuel cell (MCFC) powerplant and extended further the model with experimental validation for several load points in [25]. Uzunoglu and Alam [26] developed a hybrid fuel cell and supercapacitors dynamic model where the fuel cell model takes into account a methanol reformer (modelled by a transfer function) and an electrical fuel cell steady state characteristic; this approach is a functional approach which is well suitable to implements controllers (proportional-integral controller in this case) to control the overall system. However, in this kind of models, there is, on the one hand, the graphical part (Simulink) of the model (see [26][Fig. 2]) and, on the other hand, a file which contains all the numerical parameters. This makes the model really hard to read and it cannot be used easily by someone who wants to simply re-parametrise or improve some parts of the model.

Pasricha and Shaw [27] extended the static current voltage description to include temperature dependence with a dynamic modelling of the membrane temperature. Correa et al. [28] developed a computer-controlled high-power converter to emulate static and dynamic fuel cell characteristics: the model includes membrane temperature and humidity dependencies, efficiency, reactant flows, cooling air fans and water pump. This model has been implemented in a LabView (National instruments) environment which allows signal-flow graphical programming.

Stephanopoulou and co-workers [29–32] developed one of the most advanced control-oriented nonlinear fuel cell model until now. The model takes into account dynamic fuel cell reactant supply based on lumped-volume filling dynamics, auxiliaries' components (compressor, manifold, static air cooler, static humidifier). The fuel cell stack model is based on a functional approach and it is separated into four functionalities: the stack voltage, the cathode flow, the anode flow and the membrane hydratation. This kind of approach is very powerful and it is well suitable for control design and analysis. But it also has some drawbacks because the different functionalities are highly inter-dependents and they cannot be easily simulated separately because of feedbacks loops. One can notice that in the functional approach each functionality is a physical domain: humidity, electrical, fluidic functionalities are separated. Moreover, if a system designer wants to improve one part of the model, for example the cathode model, to take into account a new phenomena, he has to modify not only the cathode flow functionality (gas channels, supply manifold, return manifold), but also the voltage functionality. In this case, how can he knows which part of the model he has to modify or not? Which part of the voltage function corresponds to the cathode overpotential? How can he be sure he modified all what had to be modified? How can he test and prove, independently of the other parts, the validity of the new phenomena he took into account?

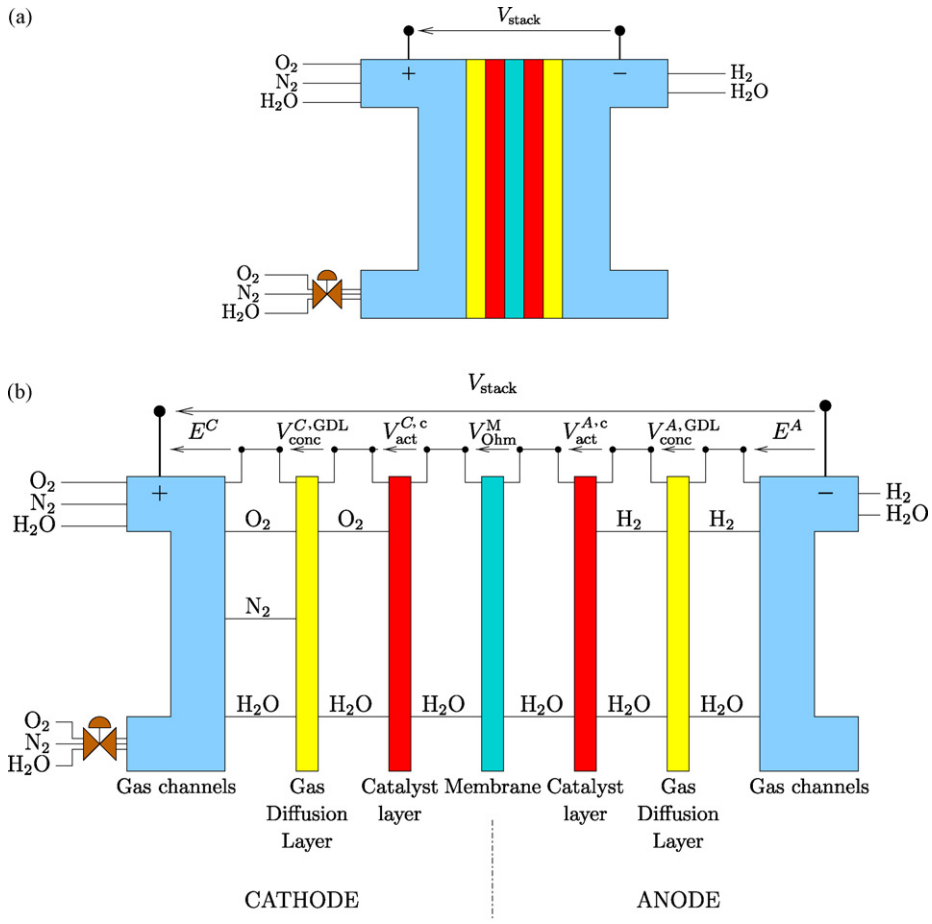

Fig. 6. Fuel cell structure abstraction levels: (a) stack level; (b) layers level.

In the structural approach, as it will be presented in the next part, these kind of problems do not arise: if the system designer wants to change the cathode model, he knows that all the multi-domain phenomena (electrical voltage, fluidic, thermal, etc.) of the cathode are taken into account in the cathode component.

2.2.2. *Top-down approach*

The modelling approach can be described by Fig. 6. Two level of abstraction are given: the first one Fig. 6(a) can be called the "stack abstraction level" where the fuel cell stack is seen only as a voltage source: in this case all the fuel cell voltage is computed in the same function taking into account the losses as it is done in many papers.

The second level (Fig. 6(b)) is more refined and can be called "layer abstraction level" because it takes into account more parts and refined phenomena. In this article, this "layer abstraction level" is used. Several structural parts are distinguished:

- The cathode gas channels: it is a simple pipe where gas can enter and leave. In this model, pressure losses are not taken into account and can be included in a more refined model;
- The cathode gas diffusion layer (GDL) where water and oxygen diffuse;
- The cathode throttle (or valve) which permits to regulate the cathode pressure;
- The cathode catalyst layer where the oxygen is consumed and the water is produced;
- The membrane where water transport phenomena are taken into account;
- The anode catalyst layer where hydrogen is consumed;
- The anode gas diffusion layer where hydrogen and water diffuse;
- The anode gas channels.

Each component imposes a voltage which can be dependent on any quantity of the component (e.g., current, partial pressure) and the overall stack voltage is obtained by plugging the components in series. Each component can be modelled, described, tested and validated *independently*.

2.2.2.1. Assumptions. In the first modelling steps, some assumptions are given. Building a more refined model will consist to remove one by one the following assumptions:

H1. Diffusion is considered in steady state.

H2. Linear diffusion (concentration gradient).

H3. No nitrogen diffusion.

H4. No pressure losses in the cathode gas channels.

H5. Hydrogen pressure is constant and perfectly regulated.

H6. Temperature is homogeneous in the entire stack.

H7. Cathode volume is constant.

H8. No water accumulation in the anode and cathode catalyst layers.

H9. Anode catalytic activity is considered so high that anode overpotential is neglected. In this case, all activation losses occur at the cathode catalyst layer.

H10. Even more or less important disparities exist between the cells of a stack, it is assumed here that n-cell stack is n times the behaviour of the equivalent mean cell. Note: there are functionalities in VHDL-AMS (`generate` function) which could permit to instantiate n cells to build an overall stack but this is not investigated here.

H11. The gases are assumed to be perfect.

H12. Water does not leave the stack in the liquid form but only in vapour form: liquid water accumulates or evaporate in the cathode gas channels [30].

According to H8 and H12, the model cannot capture electrode flooding phenomenon. The effect of excess of liquid water on oxygen mass transport rates within the cathode is really important. Two-phase flow model for PEMFCs is currently an area of active research. By neglecting this phenomenon we introduce significant errors in the results of the PEMFC cathode water distribution. It also affects the cathode overvoltage computation, making the model less realistic *in given conditions*. Most of the two-phase models are solved using CFD tools which solve spatial partial differential equations (e.g., Naviers–Stokes). An analytical model has been given by Baschuk [33] and can be added in a more refined model.

However, the tests have been performed on a low power fuel cell (1.2 kW) which works at *nearly atmospheric pressure* and a *high stoichiometry ratio* (the measured ratio is at least 5). In these conditions there are very few chances to flood electrodes of the fuel cell: the model has been validated in these conditions. In other conditions, for example at high current and low speed air stream, the model will not be able to predict water flooding.

2.2.3. Gas channels

2.2.3.1. Cathode. According to hypothesis H4, the model does not take into account pressure losses in the cathode channels. The total pressures at the inlet and outlet manifold (superscript m) $p_{\text{in}}^{\text{C,m}}$ and $p_{\text{out}}^{\text{C,m}}$, respectively, are equal to the total cathode pressure p^{C}:

$$H4 \Rightarrow p_{\text{in}}^{\text{C,m}} = p_{\text{out}}^{\text{C,m}} = p^{\text{C}} = p_{\text{O}_2}^{\text{C}} + p_{\text{N}_2}^{\text{C}} + p_{\text{H}_2\text{O}}^{\text{C}} \tag{1}$$

where $p_{\text{O}_2}^{\text{C}}$, $p_{\text{N}_2}^{\text{C}}$ and $p_{\text{H}_2\text{O}}^{\text{C}}$ are the cathode oxygen, nitrogen and vapour manifold partial pressures, respectively.

Considering all the gases as perfect gases (H11), it can be written,

$$p_i = \frac{n_i RT}{\mathcal{V}^{\text{C}}} \tag{2}$$

where p_i and n_i are the partial pressure and number of moles of the species i, respectively. $\mathcal{V}^{\text{C}}$ cathode channels volume and T is the temperature.

Derivating Eq. (2) gives,

$$\frac{\mathrm{d}\,p_i}{\mathrm{d}\,t} = \frac{RT}{\mathcal{V}^{\text{C}}}\frac{\mathrm{d}\,n_i}{\mathrm{d}\,t} + \frac{Rn_i}{\mathcal{V}^{\text{C}}}\frac{\mathrm{d}\,T}{\mathrm{d}\,t} - \frac{n_i RT}{\mathcal{V}^{\text{C}^2}}\frac{\mathrm{d}\,\mathcal{V}^{\text{C}}}{\mathrm{d}\,t} \tag{3}$$

According to H7 ($\mathrm{d}\,\mathcal{V}^{\text{C}}/\mathrm{d}\,t = 0$), the previous equation can be simplified:

$$\frac{\mathrm{d}\,p_i}{\mathrm{d}\,t} = \frac{RT}{\mathcal{V}^{\text{C}}}\frac{\mathrm{d}\,n_i}{\mathrm{d}\,t} + \frac{Rn_i}{\mathcal{V}^{\text{C}}}\frac{\mathrm{d}\,T}{\mathrm{d}\,t} \tag{4}$$

$$\frac{\mathrm{d}\,p_i}{\mathrm{d}\,t} = \frac{RT}{\mathcal{V}^{\text{C}}}\frac{1}{M_i}\frac{\mathrm{d}\,m_i}{\mathrm{d}\,t} + \frac{Rm_i}{\mathcal{V}^{\text{C}}M_i}\frac{\mathrm{d}\,T}{\mathrm{d}\,t} \tag{5}$$

where m_i and M_i are the mass and molar mass of the species i, respectively.

Each species inside the cathode channels can enter inside the channels (subscript in), go outside the fuel cell (subscript out) or go inside the catalyst layer (subscript inside). The mass balance for each species can be written,

$$\frac{\mathrm{d}\,m_i}{\mathrm{d}\,t} = q_{i,\text{in}} + q_{i,\text{out}} + q_{i,\text{inside}} \quad \text{with} \quad i \in \{\text{O}_2, \text{N}_2, \text{H}_2\text{O}\} \tag{6}$$

It has to be noticed that there are no assumption on the sign of the mass flows: the mass flows are imposed by (1) external devices like the compressor and the humidifier (2) the valve, (3) the catalyst layer and they can be either positive or negative depending on the operating point.

Eq. (5) applies for gases only whereas (6) applies for gases and liquids. The case where water is in liquid form has to be distinguished in order to take into account saturation of vapour in the air (Fig. 7).

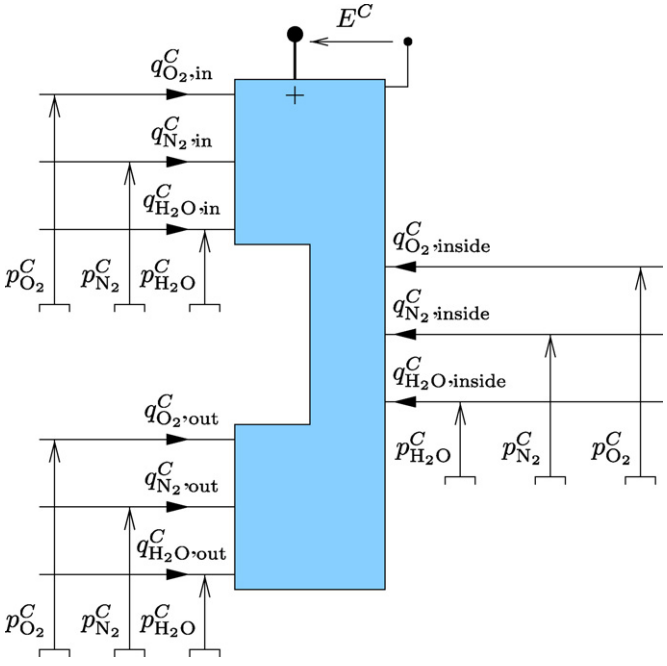

Fig. 7. Cathode gas channels.

Two equations have to be added [30]. The first one (7) checks if the total mass of water inside the control volume (gas channels) is greater than the mass of vapour which can saturate the air $m_{H_2O}^{C,Sat}$. If the total mass of vapour is lower than $m_{H_2O}^{C,Sat}$, then all the water is in the vapour form; in the other case, the air is saturated ($m_{H_2O}^{C,\mathcal{V}} = m_{H_2O}^{C,Sat}$).

The second equation (8) links the total mass of water, the vapour (subscript $\mathcal{V}$) and liquid (subscript $\mathcal{L}$) mass water.

$$m_{H_2O}^{C,\mathcal{V}} = \begin{cases} m_{H_2O}^{C} & \text{if} \quad m_{H_2O}^{C} \leq m_{H_2O}^{C,Sat} \\ m_{H_2O}^{C,Sat} & \text{elsewhere} \end{cases} \tag{7}$$

$$m_{H_2O}^{C} = m_{H_2O}^{C,\mathcal{V}} + m_{H_2O}^{C,\mathcal{L}} \tag{8}$$

The mass of water which saturates the air $m_{H_2O}^{C,Sat}$ is calculated as follows,

$$m_{H_2O}^{C,Sat} = \frac{p_{Sat}(T)\,\mathcal{V}^{C}\,M_{H_2O}}{R\,T} \tag{9}$$

where p_{Sat} is the vapour saturation pressure given by [34],

$$\begin{aligned} &\log_{10}\left(\frac{p_{Sat}(T)}{1.0\times10^{5}}\right) \\ &\quad = -2.1794 + 0.02953\,(T-273.15) \\ &\qquad - 9.1837\times10^{-5}\,(T-273.15)^{2} \\ &\qquad + 1.4454\times10^{-7}\,(T-273.15)^{3} \end{aligned} \tag{10}$$

where temperature T and pressure p_{Sat} are in Kelvin and Pascal, respectively.

Finally a set of differential equations is obtained:

$$\frac{\mathrm{d}\,p_{O_2}^{C}}{\mathrm{d}\,t} = \frac{R\,T}{\mathcal{V}^{C}}\,\frac{1}{M_{O_2}}\,\frac{\mathrm{d}\,m_{O_2}^{C}}{\mathrm{d}\,t} + \frac{R\,m_{O_2}^{C}}{\mathcal{V}^{C}\,M_{O_2}}\,\frac{\mathrm{d}\,T}{\mathrm{d}\,t} \tag{11}$$

$$\frac{\mathrm{d}\,p_{N_2}^{C}}{\mathrm{d}\,t} = \frac{R\,T}{\mathcal{V}^{C}}\,\frac{1}{M_{N_2}}\,\frac{\mathrm{d}\,m_{N_2}^{C}}{\mathrm{d}\,t} + \frac{R\,m_{N_2}^{C}}{\mathcal{V}^{C}\,M_{N_2}}\,\frac{\mathrm{d}\,T}{\mathrm{d}\,t} \tag{12}$$

$$\frac{\mathrm{d}\,p_{H_2O}^{C}}{\mathrm{d}\,t} = \frac{R\,T}{\mathcal{V}^{C}}\,\frac{1}{M_{H_2O}}\,\frac{\mathrm{d}\,m_{H_2O}^{C,\mathcal{V}}}{\mathrm{d}\,t} + \frac{R\,m_{H_2O}^{C,\mathcal{V}}}{\mathcal{V}^{C}\,M_{H_2O}}\,\frac{\mathrm{d}\,T}{\mathrm{d}\,t} \tag{13}$$

$$\frac{\mathrm{d}\,m_{O_2}^{C}}{\mathrm{d}\,t} = q_{O_2,in}^{C} + q_{O_2,out}^{C} + q_{O_2,inside}^{C} \tag{14}$$

$$\frac{\mathrm{d}\,m_{N_2}^{C}}{\mathrm{d}\,t} = q_{N_2,in}^{C} + q_{N_2,out}^{C} \tag{15}$$

$$\frac{\mathrm{d}\,m_{H_2O}^{C}}{\mathrm{d}\,t} = q_{H_2O,in}^{C} + q_{H_2O,out}^{C} + q_{H_2O,inside}^{C} \tag{16}$$

According to H3, no nitrogen diffuses from the channels to the catalyst layer that is why, in the mass conservation equation of nitrogen (15), $q_{N_2,inside}^{C}$ is not taken into account.

From the oxygen partial pressure, the fuel cell EMF cathode contribution can be computed [35]:

$$E^{C} = n\left[1.229 - 0.85\times10^{-3}(T-298.15) + \frac{RT}{2F}\ln\left(\sqrt{\frac{p_{O_2}^{C}}{101,325}}\right)\right] \tag{17}$$

2.2.3.2. Anode. The model of the anode gas channels is based on the cathode gas channels model but according to H5, it is assumed that the hydrogen partial pressure is constant. The fuel cell is in dead-end mode. Nor hydrogen, nor water can leave the fuel cell at the anode gas channels.

Considering this, it can be written:

$$m_{H_2O}^{A,\mathcal{V}} = \begin{cases} m_{H_2O}^{A} & \text{if} \ m_{H_2O}^{A} \leq m_{H_2O}^{A,Sat} \\ m_{H_2O}^{A,Sat} & \text{elsewhere} \end{cases} \tag{18}$$

$$m_{H_2O}^{A} = m_{H_2O}^{A,\mathcal{V}} + m_{H_2O}^{A,\mathcal{L}} \tag{19}$$

The mass of water which saturates the air $m_{H_2O}^{A,Sat}$ is calculated as follows,

$$m_{H_2O}^{A,Sat} = \frac{p_{Sat}(T)\,\mathcal{V}^{A}\,M_{H_2O}}{R\,T} \tag{20}$$

$$\frac{\mathrm{d}\,p_{H_2O}^{A}}{\mathrm{d}\,t} = \frac{R\,T}{\mathcal{V}^{A}}\,\frac{1}{M_{H_2O}}\,\frac{\mathrm{d}\,m_{H_2O}^{A,\mathcal{V}}}{\mathrm{d}\,t} + \frac{R\,m_{H_2O}^{A,\mathcal{V}}}{\mathcal{V}^{A}\,M_{H_2O}}\,\frac{\mathrm{d}\,T}{\mathrm{d}\,t} \tag{21}$$

$$\frac{\mathrm{d}\,p_{H_2}^{A,m}}{\mathrm{d}\,t} = 0 \tag{22}$$

$$\frac{\mathrm{d}\,m_{H_2O}^{A}}{\mathrm{d}\,t} = q_{H_2O,inside}^{A} \tag{23}$$

where $\mathcal{V}^{A}$ is the anode volume. According to H5 the hydrogen inlet mass flow $q_{H_2,in}^{A,m}$ cannot be controlled: it is imposed by the anode catalyst layer *downstream* of the anode gas channels; on the contrary, the inlet air mass flow in the cathode gas channels is imposed by the compressor and humidifier *upstream* of the gas channels.

From the hydrogen partial pressure, the fuel cell EMF anode contribution can be computed [35]:

$$E^{A} = n\,\frac{R\,T}{2\,F}\,\ln\left(\frac{p_{H_2}^{A}}{101,325}\right) \tag{24}$$

The component of the anode gas channels is given in Fig. 8.

2.2.4. Control valve or outlet throttle

Depending on the operating mode, the pressure inside the cathode can be controlled or not: the throttle opening area can be set to a constant or can be used as an extra control variable to regulate the cathode pressure [30].

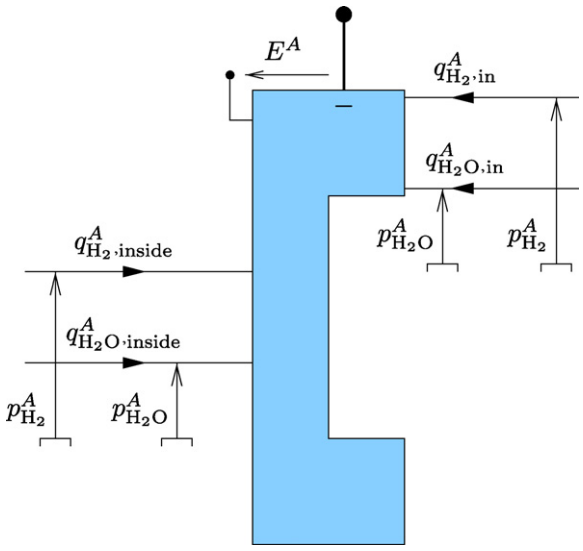

Fig. 8. Anode gas channels.

The valve or the throttle (see Fig. 9) can be modelled by a linearised form of the subcritical nozzle flow equation as given in [30], that is,

$$q^{\mathrm{V}}_{\mathrm{tot}} = k\,(p^{\mathrm{V}}_{\mathrm{tot,\,in}} - p^{\mathrm{V}}_{\mathrm{tot,\,out}}) \tag{25}$$

where $q^{\mathrm{V}}_{\mathrm{tot}}$ is the total mass flow rate going through the nozzle and $p^{\mathrm{V}}_{\mathrm{tot,\,in}}$ and $p^{\mathrm{V}}_{\mathrm{tot,\,out}}$ the inlet and outlet total pressures across the nozzle.

Three species (O_2, N_2 and H_2O) are inside the gas and the total mass flow can be written,

$$q^{\mathrm{V}}_{\mathrm{tot}} = q^{\mathrm{V}}_{\mathrm{O_2}} + q^{\mathrm{V}}_{\mathrm{N_2}} + q^{\mathrm{V}}_{\mathrm{H_2O}} \tag{26}$$

With,

$$q^{\mathrm{V}}_{\mathrm{O_2}} = \gamma_{\mathrm{O_2}}\, q^{\mathrm{V}}_{\mathrm{tot}} \tag{27a}$$

$$q^{\mathrm{V}}_{\mathrm{N_2}} = \gamma_{\mathrm{N_2}}\, q^{\mathrm{V}}_{\mathrm{tot}} \tag{27b}$$

$$q^{\mathrm{V}}_{\mathrm{H_2O}} = \gamma_{\mathrm{H_2O}}\, q^{\mathrm{V}}_{\mathrm{tot}} \tag{27c}$$

where γ_{O_2}, γ_{N_2} and γ_{H_2O} are the mass fraction of oxygen, nitrogen and vapour, respectively.

The mass fraction of the three species are computed as follows:

$$\gamma_{\mathrm{O_2}} = \frac{\chi_{\mathrm{O_2}}\, M_{\mathrm{O_2}}}{\chi_{\mathrm{O_2}}\, M_{\mathrm{O_2}} + \chi_{\mathrm{N_2}}\, M_{\mathrm{N_2}} + \chi_{\mathrm{H_2O}}\, M_{\mathrm{H_2O}}} \tag{28a}$$

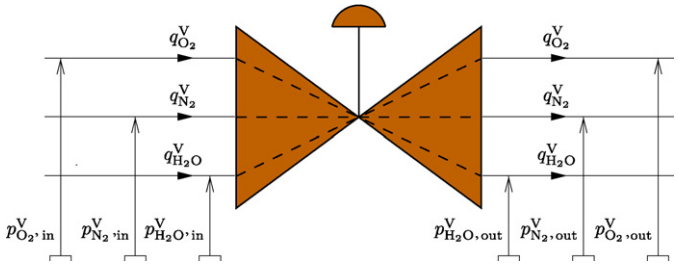

Fig. 9. Valve or throttle.

$$\gamma_{\mathrm{N_2}} = \frac{\chi_{\mathrm{N_2}}\, M_{\mathrm{N_2}}}{\chi_{\mathrm{O_2}}\, M_{\mathrm{O_2}} + \chi_{\mathrm{N_2}}\, M_{\mathrm{N_2}} + \chi_{\mathrm{H_2O}}\, M_{\mathrm{H_2O}}} \tag{28b}$$

$$\gamma_{\mathrm{H_2O}} = \frac{\chi_{\mathrm{H_2O}}\, M_{\mathrm{H_2O}}}{\chi_{\mathrm{O_2}}\, M_{\mathrm{O_2}} + \chi_{\mathrm{N_2}}\, M_{\mathrm{N_2}} + \chi_{\mathrm{H_2O}}\, M_{\mathrm{H_2O}}} \tag{28c}$$

where χ_{O_2}, χ_{N_2} and χ_{H_2O} are the mole fraction of oxygen, nitrogen and vapour, respectively.

The molar fractions computation changes if the mass flow is positive ($p^{\mathrm{V}}_{\mathrm{tot,\,in}} \geq p^{\mathrm{V}}_{\mathrm{tot,\,out}}$) or negative ($p^{\mathrm{V}}_{\mathrm{tot,\,in}} \leq p^{\mathrm{V}}_{\mathrm{tot,\,out}}$) even if in a fuel cell the mass flow should always be positive (from the cathode to the atmosphere), this case is taken into account:

$$\chi_{\mathrm{O_2}} = \begin{cases} p^{\mathrm{V}}_{\mathrm{O_2,\,in}}/p^{\mathrm{V}}_{\mathrm{tot,\,in}} & \text{if} \quad p^{\mathrm{V}}_{\mathrm{tot,\,in}} \geq p^{\mathrm{V}}_{\mathrm{tot,\,out}} \\ p^{\mathrm{V}}_{\mathrm{O_2,\,out}}/p^{\mathrm{V}}_{\mathrm{tot,\,out}} & \text{elsewhere} \end{cases} \tag{29a}$$

$$\chi_{\mathrm{N_2}} = \begin{cases} p^{\mathrm{V}}_{\mathrm{N_2,\,in}}/p^{\mathrm{V}}_{\mathrm{tot,\,in}} & \text{if} \quad p^{\mathrm{V}}_{\mathrm{tot,\,in}} \geq p^{\mathrm{V}}_{\mathrm{tot,\,out}} \\ p^{\mathrm{V}}_{\mathrm{N_2,\,out}}/p^{\mathrm{V}}_{\mathrm{tot,\,out}} & \text{elsewhere} \end{cases} \tag{29b}$$

$$\chi_{\mathrm{H_2O}} = \begin{cases} p^{\mathrm{V}}_{\mathrm{H_2O,\,in}}/p^{\mathrm{V}}_{\mathrm{tot,\,in}} & \text{if} \quad p^{\mathrm{V}}_{\mathrm{tot,\,in}} \geq p^{\mathrm{V}}_{\mathrm{tot,\,out}} \\ p^{\mathrm{V}}_{\mathrm{H_2O,\,out}}/p^{\mathrm{V}}_{\mathrm{tot,\,out}} & \text{elsewhere} \end{cases} \tag{29c}$$

The total pressure at the inlet and outlet depend also on the three species:

$$p^{\mathrm{V}}_{\mathrm{tot,\,in}} = p^{\mathrm{V}}_{\mathrm{O_2,\,in}} + p^{\mathrm{V}}_{\mathrm{N_2,\,in}} + p^{\mathrm{V}}_{\mathrm{H_2O,\,in}} \tag{30a}$$

$$p^{\mathrm{V}}_{\mathrm{tot,\,out}} = p^{\mathrm{V}}_{\mathrm{O_2,\,out}} + p^{\mathrm{V}}_{\mathrm{N_2,\,out}} + p^{\mathrm{V}}_{\mathrm{H_2O,\,out}} \tag{30b}$$

2.2.5. Catalyst layers

Catalyst layers impose the mass flow rates in function of the stack current (I). It is assumed that no pressure losses occur in the catalyst layers: the inlet and outlet vapour pressures are equal. The component of a catalyst layer is given in Fig. 10.

2.2.5.1. Cathode catalyst layer. The electrical current imposes an oxygen mass flow to the cathode gas diffusion layer (subscript GDL). The oxygen mass flow $q^{\mathrm{C,c}}_{\mathrm{O_2\,GDL}}$ taken from the cathode GDL to the cathode catalyst layer is given by

$$q^{\mathrm{C,c}}_{\mathrm{O_2,\,GDL}} = M_{\mathrm{O_2}}\,\frac{I\,n}{4\,F} \tag{31}$$

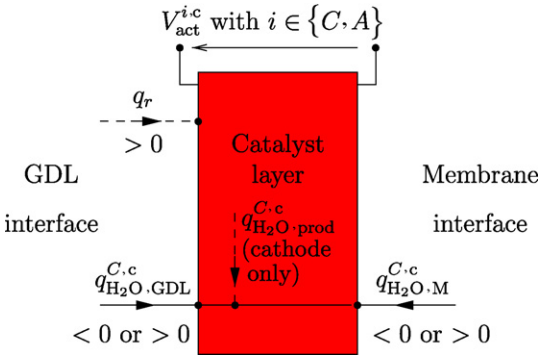

Fig. 10. Catalyst layer.

At the same time, water is produced inside the catalyst layer,

$$q^{\mathrm{C,c}}_{\mathrm{H_2O,prod}} = M_{\mathrm{H_2O}} \frac{I\,n}{2\,F} \tag{32}$$

Water vapour mass flow coming from the membrane to the catalyst layer $q^{\mathrm{C,c}}_{\mathrm{H_2O,M}}$ is not known *a priori*, it is imposed by the membrane and will be introduced in the membrane model (see Section 2.2.9).

Moreover, according to H8 no water accumulates in the catalyst layer ($\mathrm{d}\,m_{\mathrm{H_2O}}/\mathrm{d}\,t = 0$).

Water mass balance can therefore be written,

$$q^{\mathrm{C,c}}_{\mathrm{H_2O,GDL}} = -(q^{\mathrm{C,c}}_{\mathrm{H_2O,M}} + q^{\mathrm{C,c}}_{\mathrm{H_2O,prod}}) \tag{33}$$

The minus sign is to take into account mass flow conventions. If the mass flow of water produced $q^{\mathrm{C,c}}_{\mathrm{H_2O,prod}}$ at the catalyst layer is always positive, the water mass flow exchanged between the membrane and the catalyst $q^{\mathrm{C,c}}_{\mathrm{H_2O,M}}$ can be either positive (water comes from the membrane) or negative (water is absorbed by the membrane).

Activation losses occur in the catalyst layer and are computed as follows:

$$V^{\mathrm{C,c}}_{\mathrm{act}} = -n\,\mathcal{A}\,\ln\left(\frac{j}{b}\right) \tag{34}$$

where $\mathcal{A}$ and b are empirical coefficients. The current density j is defined as follows,

$$j = \frac{n\,I}{S_{\mathrm{tot}}} \tag{35}$$

where S_{tot} is the total stack active area.

2.2.5.2. Anode catalyst layer. The electrical current imposes a hydrogen mass flow to the anode gas diffusion layer (subscript GDL). The hydrogen mass flow $q^{\mathrm{A,c}}_{\mathrm{H_2\,GDL}}$ taken from the anode GDL to the anode catalyst layer is given by,

$$q^{\mathrm{A,c}}_{\mathrm{H_2,GDL}} = M_{\mathrm{H_2}} \frac{I\,n}{2\,F} \tag{36}$$

No water is produced in the anode catalyst layer. Water vapour mass flow coming from the membrane to the catalyst layer $q^{\mathrm{C,c}}_{\mathrm{H_2O,M}}$ is not known *a priori*, it is imposed by the membrane itself and will be introduced in the membrane model (see Section 2.2.9).

Moreover, according to H8 no water accumulates in the catalyst layer ($\mathrm{d}\,m_{\mathrm{H_2O}}/\mathrm{d}\,t = 0$).

Water mass balance can therefore be written,

$$q^{\mathrm{A,c}}_{\mathrm{H_2O,GDL}} = -q^{\mathrm{C,c}}_{\mathrm{H_2O,M}} \tag{37}$$

The minus sign is to take into account mass flow conventions: the water mass flow exchanged between the membrane and the anode catalyst $q^{\mathrm{A,c}}_{\mathrm{H_2O,M}}$ can be either positive (water comes from the membrane) or negative (water is absorbed by the membrane).

According H9, there are no voltage losses in the anode catalyst layer:

$$V^{\mathrm{A,c}}_{\mathrm{act}} = 0 \tag{38}$$

2.2.6. Gas diffusion layers

The relation between the current density j and the reactants molar flux J (mol cm^{-2} s^{-1}) coming from the channels to the catalyst is

$$J = \frac{j}{n_{\mathrm{e}}\,F} \tag{39}$$

where n_{e} is the number of electrons entering in the reaction.

In steady state (H1) the reactant molar flux (from channel to the catalyst) is equal to the product molar flux (from the catalyst layer to the channels).

2.2.6.1. Diffusion. The Fick law describes the diffusion as follows [19]:

$$J = -D\frac{\mathrm{d}\,c}{\mathrm{d}\,x} \tag{40}$$

where J is the diffusion molar flux, c the molar concentration and D is the diffusion coefficient.

According to H2, Eq. (40) can be written,

$$J = -D\frac{c_i(\delta) - c_i(0)}{\delta} \tag{41}$$

where $c_i(x)$ is the reactant concentration of i at abscissa x and δ is the gas diffusion layer thickness.

It has to be noticed that J can be either positive (reactant species) or negative (product species) as shown in Fig. 11.

The flux of the species i, J_i, can be computed from the mass flow q_i according to:

$$J_i = q_i\,M_i\,S_{\mathrm{tot}} \tag{42}$$

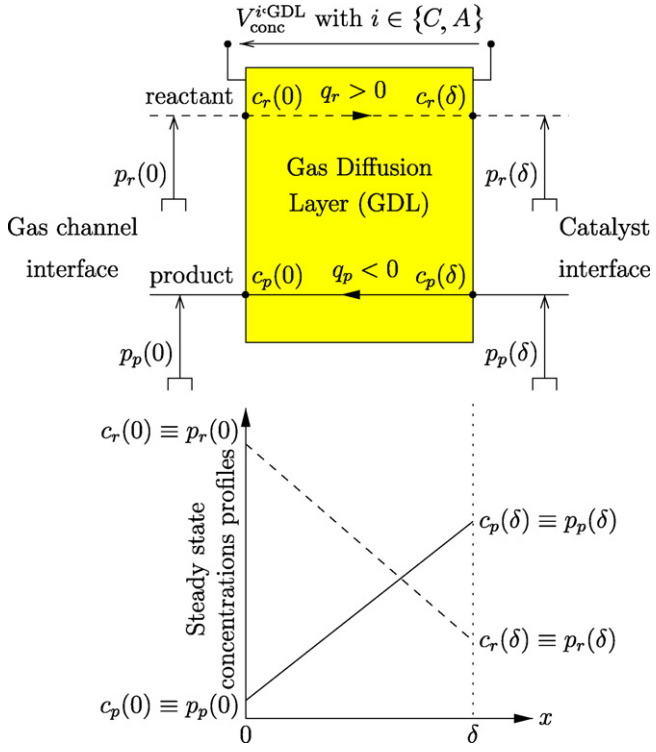

Fig. 11. Steady state reactant and product concentration profile in the gas diffusion layer.

Table 1
Critical properties of gases

Species	Molar mass	T_c (K)	p_c (atm)
H_2	2.016	33.3	12.80
Air	28.964	132.4	37.0
N_2	28.013	126.2	33.5
O_2	31.999	154.4	49.7
H_2O	18.015	647.3	217.5

where M_i is the molar mass of the species i and S_{tot} is the total active area of the stack.

Concentration profiles in steady state in the gas diffusion layer are given in Fig. 11

Concentration of the species i along the abscissa x can also be written as a function of the molar fraction $\chi_i(x)$ and the total pressure p or partial pressure $p_i(x)$,

$$c_i(x) = \frac{p}{RT}\chi_i(x) = \frac{1}{RT}p_i(x) \tag{43}$$

For low pressures, the binary diffusion coefficient D_{ij} (two species i and j) depends on the pressure and the temperature according to the following Slattery and Bird gas law [36]:

$$pD_{ij} = a\left(\frac{T}{\sqrt{T_{ci}\,T_{cj}}}\right)^{b}(p_{ci}\,p_{cj})^{1/3}\left(T_{ci}\,T_{cj}\right)^{5/12} \times \left(\frac{1}{M_i}+\frac{1}{M_j}\right)^{1/2} \tag{44}$$

where p is the total pressure (atm), D_{ij} the binary coefficient (cm^2/s) and T is the temperature (K). M_x is the molar mass of the species x, T_{cx} and p_{cx} are the critical temperature and pressure, respectively, of the species x ($x \in \{i, j\}$). The coefficients a and b differ if one of the two species is a polar gas or not (water in this case). Then,

$$a = 2.745 \times 10^{-4} \quad \text{and} \quad b = 1.823 \tag{45}$$

if the pair of gas contains nonpolar gases and

$$a = 3.640 \times 10^{-4} \quad \text{and} \quad b = 2.334 \tag{46}$$

if the pair of gas contains a polar gas (H_2O).

The critical temperatures and pressures of the different species interacting in a fuel cell are given in Table 1.

For porous media, the binary diffusion coefficient has to be corrected to account for the effects of the pore walls (porosity, tortuosity). Usually, this is accomplished by employing a modified or effective diffusivity, also known as the Bruggemann correction for the diffusion coefficients [34,19]:

$$D_{ij}^{\text{eff}} = D_{ij}\epsilon^{\tau} \;\text{ or }\; D_{ij}\frac{\epsilon}{\tau} \;\text{ for high temperatures} \tag{47}$$

where ϵ stand for the porosity of the structure (around 0.4 for fuel cell electrodes[1]) and τ is the tortuosity (from 1.5 to 10 for fuel cell electrodes) which describes the additional impedance do diffusion caused by tortuous path flow.

[1] A porosity of 0.4 means that 40% of the total electrode volume is occupied by pores. In open space, the porosity is 1 and the normal diffusion coefficient is employed.

2.2.7. Anode gas diffusion layer model

Two species, H_2 and H_2O, are present at the anode gas diffusion layer interface (hypothesis H3 permits to neglect the nitrogen diffusion) and Eq. (47) is used to compute $D^{\text{eff}}_{H_2,\,H_2O}$.

According to Eqs. (41) and (43), the partial pressures of the hydrogen and the vapour at the catalyst interface can be expressed:

$$p_{H_2}(\delta^A) = p_{H_2}(0) - \frac{J^A_{H_2}RT}{D^{\text{eff}}_{H_2,H_2O}}\delta^A \tag{48}$$

$$p_{H_2O}(\delta^A) = p_{H_2O}(0) - \frac{J^A_{H_2O}RT}{D^{\text{eff}}_{H_2,H_2O}}\delta^A \tag{49}$$

where the binary diffusion coefficient $D^{\text{eff}}_{H_2,H_2O}$ is calculated from Eqs. (44), (45) and (47).

The molar flux $J^A_{H_2}$ and $J^A_{H_2O}$ are computed from the corresponding mass flows $q^A_{H_2}$ and $q^A_{H_2O}$, respectively, with Eq. (42).

The anode concentration voltage drop is deduced from the catalyst and bulk concentrations (or partial pressures):

$$V^{A,\,GDL}_{conc} = -n\,\mathcal{C}\,\ln\left(\frac{p_{H_2}(0)}{p_{H_2}(\delta^A)}\right) \tag{50}$$

where $\mathcal{C}$ is an empirical coefficient.

2.2.8. Cathode gas diffusion layer model

Two species, O_2 and H_2O are present at the cathode gas diffusion layer interface (hypothesis H3 permits to neglect the nitrogen diffusion) and Eq. (47) is used to compute $D^{\text{eff}}_{O_2,\,H_2O}$.

According to Eqs. (41) and (43), the partial pressures of oxygen and vapour at the catalyst interface can be expressed:

$$p_{O_2}(\delta^C) = p_{O_2}(0) - \frac{J^C_{O_2}RT}{D^{\text{eff}}_{O_2,H_2O}}\delta^C \tag{51}$$

$$p_{H_2O}(\delta^C) = p_{H_2O}(0) - \frac{J^C_{H_2O}RT}{D^{\text{eff}}_{O_2\,H_2O}}\delta^C \tag{52}$$

where the binary diffusion coefficient $D^{\text{eff}}_{O_2,H_2O}$ is calculated from Eqs. (44), (45) and (47).

The cathode concentration voltage drop is deduced from the catalyst and bulk concentrations (or partial pressures):

$$V^{C,\,GDL}_{conc} = -n\,\mathcal{C}\,\ln\left(\frac{p_{O_2}(0)}{p_{O_2}(\delta^C)}\right) \tag{53}$$

2.2.9. Membrane

The membrane model (see Fig. 12) developed here is the Springer isothermal and one-dimensional model given in [34] where the authors empirically determine relationships correlating membrane conductivity and electrode porosity with water content in the Nafion membrane.

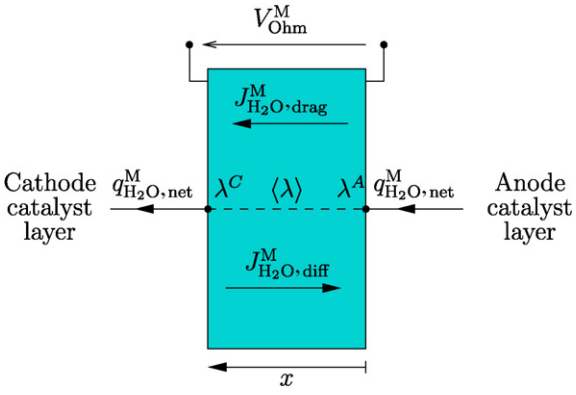

Fig. 12. Membrane.

The membrane resistance is deduced from its conductivity. Since membrane conductivity is highly dependent on its water content, it is essential to know how water content varies across a Nafion membrane. Two opposite phenomena occur in the membrane and have to be taken into account: the electro-osmotic drag and the back diffusion of water.

2.2.9.1. Water content of the membrane. The water content λ in a Nafion membrane is not uniform as it will be shown in next parts. It is defined as the ratio of the number of water molecules to the number of charged sites. Experimental results show that λ can varies from 0 (completely dehydrated membrane) to 22 (full saturation, under certain conditions) [19]. In order to compute the water profile in the membrane, boundary conditions have to be known. The water content is related to the water activity on the faces of the membranes according to the following law [34]:

$$\lambda = \begin{cases} 0.043 + 17.81\,a_{H_2O} - 39.85\,a_{H_2O}^2 + 36.0\,a_{H_2O}^3 & \text{if } 0 < a_{H_2O} \le 1 \\ 14 + 1.4(a_{H_2O} - 1) & \text{if } 1 < a_{H_2O} \le 3 \end{cases} \quad (54)$$

These values are given for a temperature of 30 °C but it has been assumed in [34] that it is valid also up to 80 °C.

The water activity is calculated from the partial water pressure p_{H_2O} and saturation pressure p_{Sat}:

$$a_{H_2O} = \frac{p_{H_2O}}{p_{Sat}(T)} \quad (55)$$

where the vapour saturation pressure p_{Sat} is given by Eq. (10).

From the boundary water partial pressure conditions at the cathode (superscript C) and anode (superscript A), the average Nafion water content can be found:

$$\langle\lambda\rangle = \frac{\lambda^{C} + \lambda^{A}}{2} \quad (56)$$

where λ^{C} is found from the water partial pressure at the cathode GDL side and λ^{A} from the water partial pressure at the anode GDL side using Eq. (54).

2.2.9.2. Electro-osmotic drag. The protons travelling through the pores of the Nafion membrane (from the anode to the cathode) generally drag one ore more water molecules along with them. The degree to which movement causes water movement is quantified by the electro-osmotic drag coefficient n_{drag}, which is defined as the number of water molecules accompanying the movement of each proton [19]. It is commonly assumed that n_{drag} varies linearly with λ as [34]:

$$n_{drag} = n_{drag}^{Sat}\,\frac{\lambda}{22} \quad \text{for } 0 \le \lambda \le 22 \quad (57)$$

where $n_{drag}^{Sat} \approx 2.5$ is the electro-osmotic drag coefficient in fully hydrated Nafion.

Other drag coefficients expressions have been reported in the literature [37,38] but Eq. (57) have been widely used [30,34] and have shown good results.

The water drag flux $J^{M}_{H_2O,\,drag}$ (mol cm^{-2} s^{-1}) from anode to cathode as a function of the current density j (A cm^{-2}) and electro-osmotic drag coefficient n_{drag} is given by

$$J^{M}_{H_2O,\,drag} = 2\,n_{drag}\,\frac{j}{2\,F} \quad (58)$$

2.2.9.3. Back diffusion of water. When the concentration of water at the cathode side is higher than the one at the anode side, water diffuses back from the cathode to the anode. This phenomenon counterbalances the effect of the electro-osmotic drag. The water back-diffusion flux can be determined by [34]:

$$J^{M}_{H_2O,\,diff} = -\frac{\rho_{dry}}{M_m}\,D_\lambda\,\frac{d\lambda}{dx} \quad (59)$$

where ρ_{dry} is the Nafion dry density ($\rho_{dry} = 0.00197\,kg/m^3$ [19]), M_m is the Nafion equivalent weight ($M_m = 1.0\,kg/mol$ [19]) and x is the direction through the membrane thickness from the anode to the cathode.

The water diffusivity D_λ (cm^2/s) is not constant; it depends on the temperature T and water content λ of the membrane according the following law [34]:

$$D_\lambda = 10^{-6}\,\exp\left[2416\left(\frac{1}{303} - \frac{1}{T}\right)\right](2.563 - 0.33\lambda + 0.0264\lambda^2 - 0.000671\lambda^3) \quad \text{for } \lambda > 4 \quad (60)$$

As for the drag coefficients, other expression of the Nafion diffusivity has been published [39]. Eq. (60) is valid only if λ is greater than 4; if λ is lower than for other expressions of the Nafion diffusivity can be found [30] but it corresponds to working points where the membrane is severely dehydrated.

2.2.9.4. Water mass balance. Combining Eqs. (58) and (59) the total water flux in Nafion is given:

$$J^{M}_{H_2O,\,net} = 2\,n_{drag}\,\frac{j}{2\,F} - \frac{\rho_{dry}}{M_m}\,D_\lambda\,\frac{d\lambda}{dx} \quad (61)$$

As proposed in [34,19], the previous equation can be rearranged setting $J^{M}_{H_2O,\,net} = \alpha\,j/(2\,F)$ where α is unknown and denotes the ratio of water flux in the membrane to hydrogen flux:

$$\frac{d\lambda}{dx} = \left(2\,n_{drag}^{Sat}\,\frac{\lambda}{22} - \alpha\right)\,\frac{j\,M_m}{2\,F\,\rho_{dry}\,D_\lambda} \quad (62)$$

From Eq. (42), the total water mass flow (kg s^{-1}) in Nafion is,

$$q^{\mathrm{M}}_{\mathrm{H_2O,\,net}} = M_{\mathrm{H_2O}}\, J^{\mathrm{M}}_{\mathrm{H_2O,\,net}}\, S_{\mathrm{tot}} = M_{\mathrm{H_2O}}\, \alpha\, \frac{j}{2\,F}\, S_{\mathrm{tot}} \tag{63}$$

In the ordinary differential equation (62) there are two unknowns, λ and α. This equation cannot be solved analytically since D_λ is a function of λ. However, if D_λ does not change too much with λ when λ is greater than 4.0 (it is assumed to be constant in [30]), an estimation of D_λ can be found and Eq. (62) can be solved analytically.

The water diffusivity in the Nafion is calculated as follows:

$$D_\lambda \approx D_{\langle\lambda\rangle} \tag{64}$$

where $\langle\lambda\rangle$ is the average water content in the membrane given by Eq. (56).

Solving Eq. (62), λ profile in the membrane can be found:

$$\lambda(x) = \frac{11\,\alpha}{n^{\mathrm{Sat}}_{\mathrm{drag}}} + \mathcal{C}\,\exp\left(\frac{j\,M_{\mathrm{m}}\,n^{\mathrm{Sat}}_{\mathrm{drag}}}{22\,F\,\rho_{\mathrm{dry}}\,D_{\langle\lambda\rangle}}x\right) \tag{65}$$

The two unknowns α and $\mathcal{C}$ (integration constant) can be found from the two boundary conditions $\lambda(0)$ and $\lambda(\delta^{\mathrm{M}})$ which are computed from Eq. (54).

2.2.9.5. Membrane-specific resistance and voltage drop. The Nafion conductivity σ^{M} (S cm^{-1}) is given by [34]:

$$\sigma^{\mathrm{M}}(T,\lambda) = \sigma_{303\,\mathrm{K}}(\lambda)\,\exp\left[1268\,\left(\frac{1}{303} - \frac{1}{T}\right)\right] \tag{66}$$

where

$$\sigma_{303\,\mathrm{K}}(\lambda) = \sigma_1\,\lambda - \sigma_2 \tag{67}$$

where $\sigma_1 = 0.005193$ and $\sigma_2 = 0.00326$.

The membrane-specific resistance r^{M} (Ω cm^{-2}) is obtained by integrating the local resistance over the membrane thickness δ^{M} (cm):

$$r^{\mathrm{M}} = \int_0^{\delta^{\mathrm{M}}} \frac{\mathrm{d}\,x}{\sigma^{\mathrm{M}}(T,\lambda(x))} \tag{68}$$

Finally, after integrating Eq. (68):

$$\begin{aligned} r^{\mathrm{M}} = {} & \frac{2\,\exp[1268((1/T)-(1/303))]}{j\,M_{\mathrm{m}}(22\,\sigma_1\,\alpha - 2\,\sigma_2\,n^{\mathrm{Sat}}_{\mathrm{drag}})}\Big[-22\,F\rho_{\mathrm{dry}}\,D_{\langle\lambda\rangle} \\ & \ln(22\,\sigma_1\,\alpha + 2\,\sigma_1\,\mathcal{C}\,n^{\mathrm{Sat}}_{\mathrm{drag}}\mathrm{e}^{\delta^{\mathrm{M}}\,j\,M_{\mathrm{m}}\,(n^{\mathrm{Sat}}_{\mathrm{drag}}/22\,F\,\rho_{\mathrm{dry}}\,D_{\langle\lambda\rangle})} \\ & -2\,\sigma_2\,n^{\mathrm{Sat}}_{\mathrm{drag}}) - \delta^{\mathrm{M}}\,j\,n^{\mathrm{Sat}}_{\mathrm{drag}} + 22\,F\,\rho_{\mathrm{dry}}\,D_{\langle\lambda\rangle} \\ & \ln(22\,\sigma_1\,\alpha + 2\,\sigma_1\,\mathcal{C}\,n^{\mathrm{Sat}}_{\mathrm{drag}} - 2\,\sigma_2\,n^{\mathrm{Sat}}_{\mathrm{drag}})\Big] \end{aligned} \tag{69}$$

The membrane thickness depends on the membrane type, they are summarised in Table 2.

The voltage drop across the membrane is simply deduced from the membrane-specific resistance r^{M} and the current density j from the Ohm law:

$$V^{\mathrm{M}}_{\mathrm{Ohm}} = -n\,r^{\mathrm{M}}\,j \tag{70}$$

Table 2
Nafion membrane types (thickness)

Name	δ^{M} (mil)	δ^{M} (μm)
Nafion 117	7	178
Nafion 115	5	127
Nafion 112	2	51

3. Results and discussion

The simulation of the model has been performed under both *Smash* from Dolphin Integration and *Simplorer* from Ansoft. Simplorer proposes optimisation functionalities like the Simplex or Genetic Algorithms which have been used to identify the model parameters of the Nexa module from Ballard.

The identification method is shown in Fig. 13: experimental data have been imported in the simulation tool (2D look-up tables). Experimental measurements of the temperature (the model does not take into account temperature dynamics), current and air mass flow feed the model: experimental and simulated voltages are compared. The squared voltage error is integrated along all the cycle: it is the objective function to minimise by varying parameters (S_{tot}, $\mathcal{A}$, b, $\mathcal{C}$, $\mathcal{V}^{\mathrm{C}}$, $\mathcal{V}^{\mathrm{A}}$).

Because the Nexa module is a closed-loop system and all the data, like the humidity of the air, are not known, it has been assumed that the cathode and anode volumes are equal and that the cathode is perfectly humidified, that is, $p_{\mathrm{H_2O}}(\mathrm{C}) = p_{\mathrm{Sat}}$.

A parameter sweep analysis has been performed around the solution given by the optimisation. The integral quadratic error has been plotted vs. each parameter variation around the optimal solution in Fig. 14.

As shown in the figures, three parameters (activation losses parameters and total active surface area) have an influence on the integral of the quadratic error. Moreover it can be seen that the obtained solution is optimal: each of the three parameters obtained by means of the optimisation is at the minimum of the error.

However, two parameters (the concentration losses coefficient $\mathcal{C}$ and volumes of the cathode and anode $\mathcal{V}$) have nearly no influence on the error. The explanations are different for each parameter:

- *The concentration losses coefficient*: The fuel cell used to validate the model does not allow to work at high currents (with possibly low stoichiometry ratio) where the concentration losses become predominant. In the conditions where the tests have been performed the concentration losses are not significant enough to show any influence on the fuel cell stack voltage. To identify this parameter tests should be performed at higher currents and lower air stream (*i.e.*, lower air stoichiometry ratio) to decrease the partial pressure of oxygen inside the GDL. These tests cannot be performed on the Nexa module because the system enters emergency when the partial pressure of oxygen drops.
- *The cathode and anode volumes*: The Nexa module works at a nearly atmospheric pressure with open-mode cathode. There is no pressure valve to control the pressure inside the

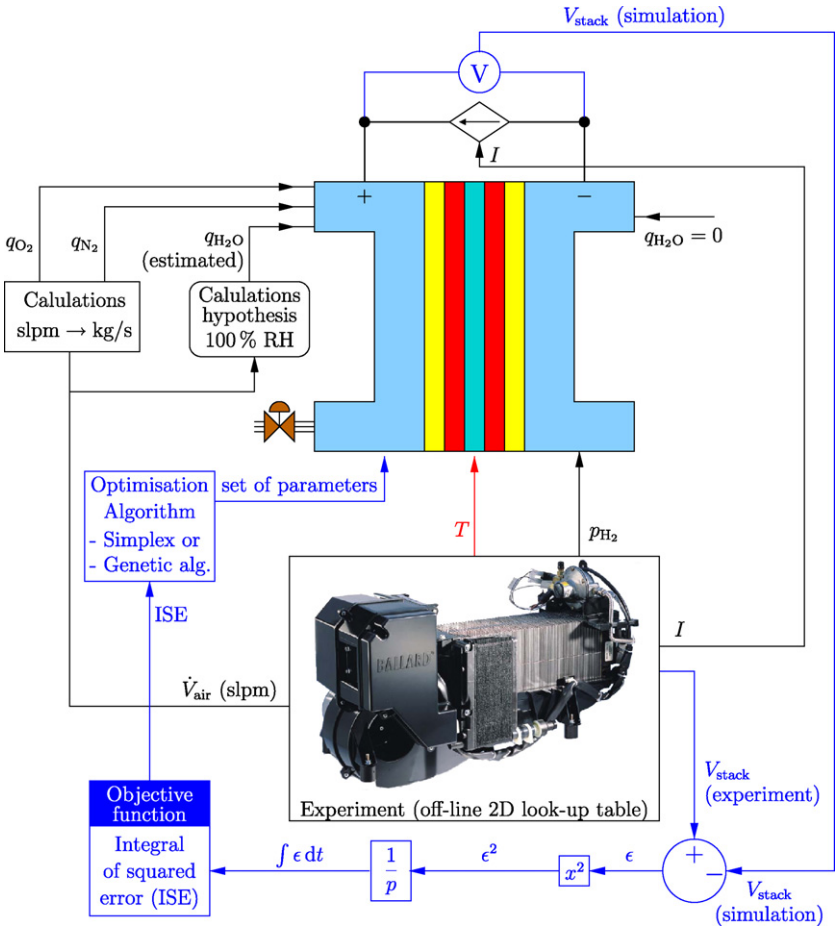

Fig. 13. Parameters identification method.

cathode gas channels. This means that the pressure dynamics is not really high for an air flow change and the pressure stays roughly around the atmospheric pressure. To identify this parameter, tests should be performed on a high pressure (around 2–3 bar) fuel cell stack where air flow changes have a bigger influence on the pressure dynamics.

Fig. 15 shows the experimental current profile which has been used to feed the model. The experimental and simulated voltages are plotted in Fig. 16: it can be seen that the model fits quite well to the experimental results. Some differences between the model and the simulation are relatively big at low current. These differences could be explained by the assumption that the cathode channels are saturated: the Nexa humidity and heat exchanger time response is not known and can have an influence on the water content of the inlet air. The big time transients in the voltage between 1500 s and 2000 s can be explained by the time constant of the humidifier and/or the time constant of the membrane water content: the membrane model is assumed to be in steady state. A more refined model has to be built to take into account this phenomena.

However, most of the voltage errors between the model and experiment appear for low current: they do not have a big influence on the simulated power as seen in Fig. 17. The experimental and simulated powers show very good agreement: this model can consequently be used with power converters or other energy sources in a fuel cell system for power applications like the one from [26].

The membrane-specific resistance depends on the temperature (Fig. 18), the membrane water content (Fig. 19) and current density as seen in (69). Mann et al. [40] proposed an empirical expression for the specific membrane resistance (see Fig. 20) and the results predicted by Eq. (69) show good agreements with the Mann's formula. It can be seen in Fig. 20 that the specific resistance is not constant and cannot be considered constant as it is proposed in a great deal of papers. For example, at the beginning of the simulation, the specific resistance is equal to $80\,\Omega\,cm^{-2}$ and at 1500 s where the current is the same (see Fig. 15) the specific resistance is lower than $60\Omega\,cm^{-2}$ because the water content of the membrane and the temperatures are different.

According to the resistance evolution, the voltage should decrease between 1700 s and 2000 s. However, the current is really low and the effect of the resistance on the voltage is not predominant. The water content at the cathode side is decreasing thanks to the temperature: the partial pressure of water inside the cathode gas channel decreases and consequently the partial pressure of oxygen is slightly increasing. According to the Nernst equation, if the oxygen partial pressure increases, the voltage increases: this phenomenon explains the small increase of the stack voltage between 1700 s and 2000 s.

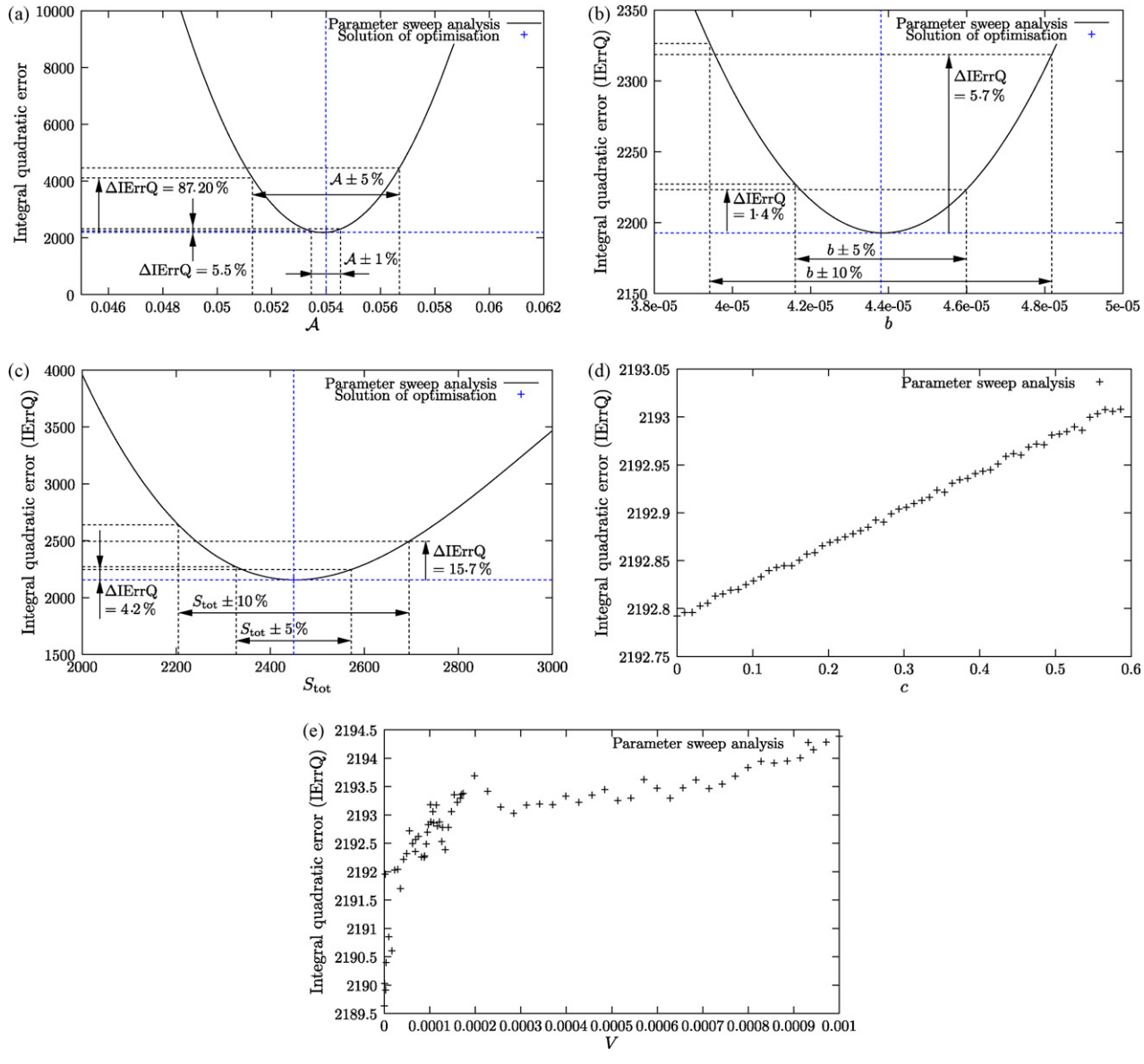

Fig. 14. Parameters sensitivity analysis: (a) $\mathcal{A}$; (b) b; (c) S_{tot}; (d) $\mathcal{C}$; (e) $\mathcal{V}$.

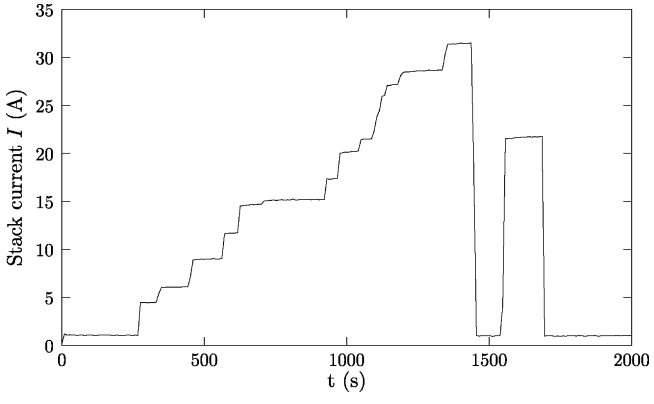

Fig. 15. Experimental stack current.

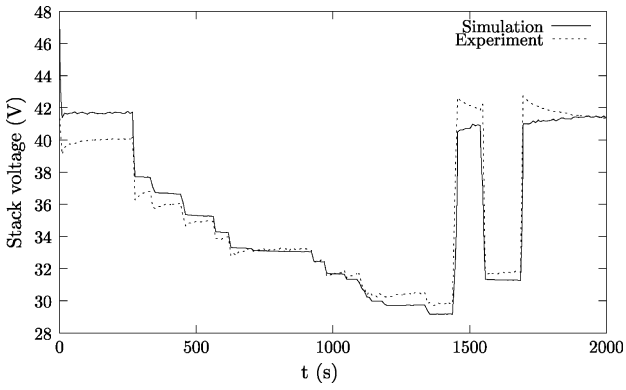

Fig. 16. Experimental and simulated voltages.

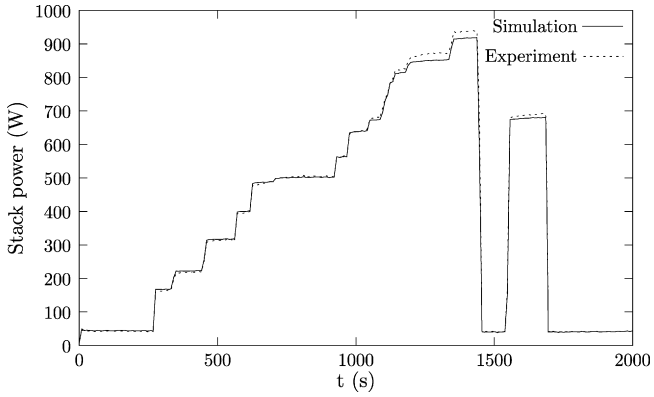

Fig. 17. Experimental and simulated power.

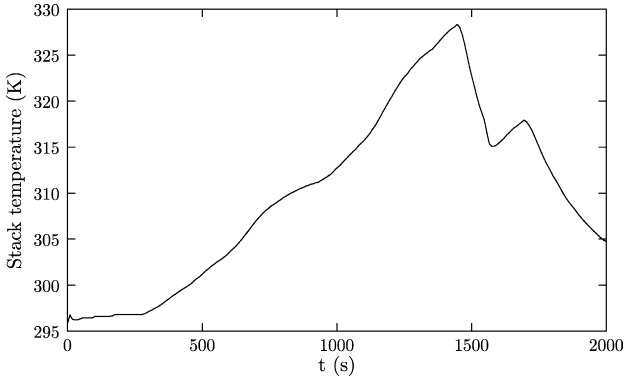

Fig. 18. Experimental stack temperature.

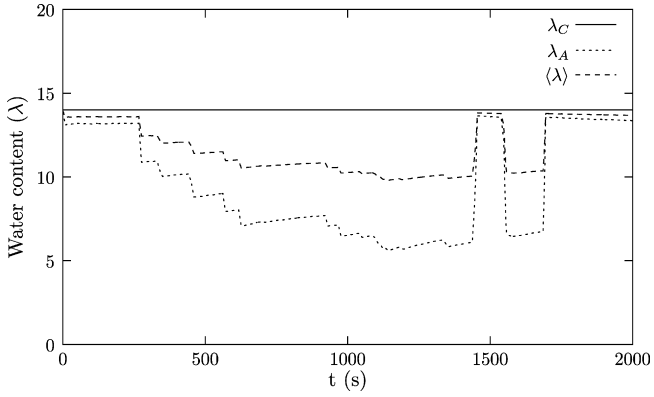

Fig. 19. Water content across the membrane and average membrane water content.

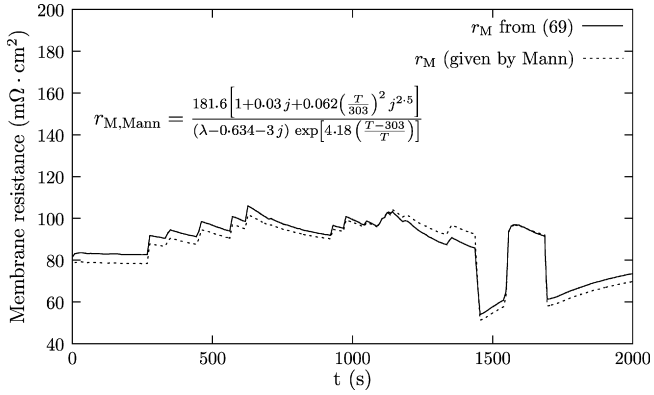

Fig. 20. Simulated membrane-specific resistance with comparison with resistance given by Mann et al. [40,41].

4. Conclusion

This study presents a VHDL-AMS modelling of a complex multi-domain energy conversion system: a fuel cell stack. A comparative study between the different modelling approaches (bond graphs, electrical equivalent circuits) is given to show the great advantages of the VHDL-AMS language in the design process of fuel cell systems. The fuel cell model includes the water transport in the membrane.

The fuel cell stack model fits the experimental results and the VHDL-AMS-based modelling approach shows its powerful capabilities on a fuel cell model, which is a complex multi-domain energy system. The presented model is able to predict the voltage and the power of the fuel cell with a good accuracy taking into account the water content of the membrane. This last point is really important to design the air supply system (compressor and humidifier) and its associated control.

The modelling approach allows the design team to split the work into several parts (concurrent engineering) and validate each part independently. This work is a first step in building a complete VHDL-AMS model of a fuel cell system including auxiliaries and power converters. The next steps will consist in improving the fuel cell stack model by including its thermal behaviour and the electrodes flooding phenomenon, which has to be accounted for if some working conditions are considered (high current density and low stoichiometry ratio). Finally, the fuel cell stack auxiliaries and the power converters will be modelled. Once the model of each sub-part has been built and validated, the complete system can be assembled. The fuel cell system virtual prototype will help the designers determine the optimal design of the system (hybridization with supercapacitors, batteries, etc.) and its optimal control before its implementation on a real fuel cell system.

References

[1] B. Blunier, A. Miraoui, Piles combustible, Principe, modélisation et applications avec exercices et problèmes corrigés, Technosup, 2007 (book in French).
[2] Y. Hervé, P. Desgreys, Forum on Design Languages, FDL'06, 2006, pp. 69–76.
[3] E. Christen, K. Bakalar, IEEE Trans. Circuit Syst. II: Analog Digital Signal Process. 46 (10) (1999) 1263–1272.
[4] F. Pêcheux, C. Lallement, A. Vachoux, IEEE Trans. Comput. Des. Integrat. Circuit Syst. 24 (24) (2005) 204–225.
[5] IEEE, 1076.1.1 IEEE Standard VHDL Analog and Mixed-Signal Extensions—Packages for Multiple Energy Domain Support, IEEE Computer Society, June 2005.
[6] P.J. Ashenden, G.D. Peterson, D.A. Teegarden, The System Designer's Guide to VHDL-AMS, Analog Mixed Signal and Mixed-Technology Modeling, Morgan Kaufmann Publishers, 2003.
[7] E. Moser, N. Mittwollen, Proceedings of the Design, Automation and Test in Europe 1998, 1998, pp. 59–63.
[8] D.M. Bernardi, M.W. Verbrugge, J. Electrochem. Soc. 139 (9) (1992) 2477–2491.
[9] D. Cheddie, N. Munroe, J. Power Sources 147 (2005) 72–84.
[10] A. Biyikoglu, Int. J. Hydrogen Energy 30 (2005) 1181–1212.
[11] R. Saisset, C. Turpin, S. Astier, B. Lafage, Proceedings of the Power Electronics Specialists Conference 2002. pesc 02. 2002 IEEE 33rd Annual, vol. 1, 2002, pp. 327–332.

[12] S. Benbouzid, G. Dauphin-Tanguy, F. Guillemard, C. Nouillant, Proceedings of the International Conference on Vehicle Power and Propulsion, IEEE VPP'04, 2004.
[13] R. Saisset, G. Fontes, C. Turpin, S. Astier, J. Power Sources 156 (2006) 100–107.
[14] P. Famouri, R. Gemmen, Proceedings of the Power Engineering Society General Meeting 2003, IEEE, vol. 3, 2003.
[15] D. Yu, S. Yuvarajan, Proceedings of the Applied Power Electronics Conference and Exposition, APEC '04, vol. 1, 2004, pp. 362–366.
[16] J. Larminie, Proceedings of the IEE Colloquium on Electrochemical Measurement, 1994, pp. 12/1–126/126.
[17] J.C. Amphlett, R.F. Mann, B.A. Peppley, P.R. Roberge, A. Rodrigues, J. Power Sources 61 (1996) 183–188.
[18] F. Barbir, PEM Fuel Cells, Environmental Engineering, Elsevier Academic Press, 2005.
[19] R.P. O'Hayre, S.-W. Cha, W. Colella, F.B. Prinz, Fuel Cell Fundamentals, John Wiley & Sons, Inc., 2006.
[20] K. Runtz, M. Lyster, Canadian Conference on Electrical and Computer Engineering 2005, 2005, pp. 794–797.
[21] E. Hernandez, B. Diong, Applied Power Electronics Conference and Exposition, APEC 2005, vol. 1, 2005, pp. 121–126.
[22] C. Wang, M. Nehrir, S. Shaw, IEEE Trans. Energy Conv. 20 (2) (2005) 442–451.
[23] C. Wang, M. Nehrir, H. Gao, IEEE Trans. Energy Conv. 21 (2) (2006) 586–595.
[24] M. Lukas, K. Lee, H. Ghezel-Ayagh, IEEE Trans. Energy Conv. 14 (4) (1999) 1651–1657.
[25] M. Lukas, K. Lee, H. Ghezel-Ayagh, IEEE Trans. Energy Conv. 16 (3) (2001) 289–295.
[26] M. Uzunoglu, M. Alam, IEEE Trans. Energy Conv. 21 (3) (2006) 767–775.
[27] S. Pasricha, S. Shaw, IEEE Trans. Energy Conv. 21 (2) (2006) 484–490.
[28] J. Correa, F. Farret, J. Gomes, M. Simoes, IEEE Trans. Ind. Appl. 39 (4) (2003) 1136–1142.
[29] J. Pukrushpan, A. Stefanopoulou, H. Peng, Proceedings of the 2002 American Control Conference 2002, vol. 4, 2002, pp. 3117–3122.
[30] J.T. Pukrushpan, A.G. Stefanopoulou, H. Peng, Control of Fuel Cell Power Systems: Principle, Modeling Analysis and Feedback Design, Advances in Industrial Control, 2004, ISBN: 1852338164.
[31] J. Pukrushpan, A. Stefanopoulou, H. Peng, IEEE Control Syst. Mag. 24 (2) (2004) 30–46.
[32] A. Vahidi, A. Stefanopoulou, H. Peng, IEEE Trans. Control Syst. Technol. (2006) 1047–1057.
[33] J. Baschuk, L. Xianguo, J. Power Sources 86 (2000) 181–196.
[34] T.E. Springer, S. Zawodzinski, S. Gottesfeld, J. Electrochem. Soc. 138 (8) (1991) 2334–2342.
[35] J. Larminie, A. Dicks, Fuel Cell Systems Explained, Second ed., Wiley, 2003.
[36] J.C. Slattery, R.B. Bird, AIChE 4 (1958) 137–142.
[37] T. Fuller, J. Newmann, J. Electrochem. Soc. 139 (1992) 1332.
[38] T.A. Zawodzinski, T.E. Springer, J. Davey, R. Jestel, C. Lopez, J. Valerio, S. Gottesfeld Jr., J. Electrochem. Soc. 140 (7) (1993) 1981–1985.
[39] S. Motupally, A.J. Becker, J.W. Weidnera, J. Electrochem. Soc. 147 (9) (2000) 3171–3177.
[40] R.F. Mann, J.C. Amphlett, M.A. Hooper, H.M. Jensen, B.A. Peppley, P.R. Roberge, J. Power Sources 86 (2000) 173–180.
[41] F.A. Farret, M.G. Simoes, Integration of Alternative Sources of Energy, First ed., Wiley–IEEE Press, 2006, ISBN: 0471712329.